Proceedings of the 15th International Symposium on Unsteady Aerodynamics, Aeroacoustics & Aeroelasticity of Turbomachines
ISUAAAT15
24-27 September 2018, University of Oxford, UK

ISUAAAT15-048

AN INVERSE APPROACH TO IDENTIFY TUNED AERODYNAMIC DAMPING, SYSTEM FREQUENCIES AND MISTUNING. PART 1: THEORY AND BENCHMARK UNDER ROTATING CONDITIONS

Felix Figaschewsky **Arnold Kühhorn**
Chair of Structural Mechanics and Vehicle Vibration Technology
Brandenburg University of Technology Cottbus-Senftenberg
Cottbus, Brandenburg, Germany

ABSTRACT

The overall objective of this work is to present a novel approach for the identification of system properties of mistuned rotors from measurements under operating conditions. The system properties of interest are: tuned overall damping values as a function of the inter-blade phase angle (IBPA), natural frequencies as a function of the travelling wave mode (TWM) index, mistuning distributions and the force amplitudes as a function of the TWM index. The scope of this part is limited to the theory and a numerical benchmark under rotating conditions. After the theoretical basis is provided, a minimum example is treated with the basic algorithm revealing the necessity of stabilisation techniques. The stabilised approach is applied to 2 simulated blade tip timing (BTT) data sets (clean and erroneous) to demonstrate the suitability of the methodology.

INTRODUCTION

In the recent decades many effort has been spent to understand the vibrational behaviour of mistuned bladed rotors under a multitude of operating conditions and with varying degree of complexity. Nevertheless, the agreement of measured with predicted responses is sometimes unsatisfactory. Due to the plurality of influencing factors it is often not obvious which assumption, simplification or modelling technique is responsible for the remaining discrepancies. Typical uncertainties in structural analyses are the influence of boundary conditions (clamped vs. free, single rotor vs. shaft assembly, etc.) or operating conditions (pressure/temperature loads, centrifugal loads, the Coriolis effect, etc.). The aerodynamic model also suffers from a certain impact of the chosen boundary conditions (reflecting vs. non-reflecting, etc.), the impact of the modelling technique (time vs. frequency domain, linear vs. non-linear, viscid vs. inviscid, one equation vs. multiple equation turbulence model, influence coefficient technique vs. phase lagged boundaries, etc.) and the impact of the degree of detail (single stage flutter vs. embedded flutter, secondary flows in gaps, shroud cavities, bleed ports, etc.). Finally, the chosen coupling approach (decoupled vs. fully coupled) and the mistuning model as well as the applied mistuning distribution can also cause mismatches. Since all these influences superpose in a simple comparison of the measured vibration amplitudes of the blades, this work aims at extracting as much information as possible from measurements of the blade vibration. This information can then be used to identify which part of the model needs to be improved. Within the recent years different approaches for the identification of mistuning at rest have been developed (indirect methods like the FMM-ID [1–3], direct methods based on detuning [4] or geometry [5, 6]). However, these are not applicable to measurements under operating conditions where sometimes the frequency at which the maximum response of a blade occurs is utilized as an approximation of the mistuning distribution. A direct measurement of the aerodynamic force is currently not possible since this would require a huge number of unsteady pressure measurements. In terms of the forcing function, it is not only the amount of force in the dominant TWM that matters but also any additional excitation of further TWMs, e.g. due to rotor-stator interaction (Tyler-Sofrin modes). The direct measurement of the tuned system's natural frequencies is also not possible, since every manufactured rotor can be regarded as mistuned. The FMM-ID [1–3] approach is an indirect approach that is able to derive these quantities. However, the drawback of the FMM-ID is, that it processes mistuned natural frequencies and mode shapes which need to be derived by a non-linear curve fitting software. Due to the non-linear property of the algorithm different solutions can be obtained depending on the weighting technique and initial values –

especially for those cases where many close system modes interact with each other, e.g. for fundamental blade modes with stiff disks, many blades and high damping ratios. The presented approach aims at avoiding this issue by processing the measured blade individual frequency response functions (FRFs) directly. Furthermore, the introduced approach aims at deriving the tuned damping ratios rather than the mistuned ones like within the FMM-ID [1–3] or other approaches [7]. This is due to the fact, that common methods for the prediction of aerodynamic damping produce tuned aerodamping vs. IBPA curves which can then be directly compared to what has been extracted from the measurement. Hence, the proposed methodology offers a great potential for the validation of CFD codes and techniques with data obtained for real industrial components operating in the proper environment. Usually, this validation can only be done by comparing predictions with measurements of simple, usually non-rotating cascades with prescribed torsion or flap motion [8, 9].

NOMENCLATURE

c_j	Stiffness scaling of sector j
$\mathbf{D}$	Damping matrix
$\mathbf{d}$	Vector of unknown damping values
$\mathbf{E}$	Transformation matrix of complex DFT
$\underline{\mathbf{f}}$	Vector of unknown modal force amplitudes
$\hat{\underline{\mathbf{f}}}_j$	Vector of force amplitudes on j-th blade
$\underline{\mathbf{g}}$	Vector of unknown mistuning
$\underline{i}$	Imaginary unit
j	Blade index
k	TWM index
$\mathbf{K}$	Stiffness matrix
$\mathbf{L}$	Least squares matrix
$\mathbf{M}$	Mass matrix
m	Mode index
N	Number of blades
N_f	Number of measured frequency lines
$\mathbf{P}$	Projection vector
$\hat{\underline{q}}_m$	Complex modal amplitude of m-th mode
$\overline{\underline{q}}_m$	TWM expansion of generalised displacement
s	Frequency index
$\mathbf{w}$	Vector of unknown system frequencies
$\mathbf{x}_j$	Displacement vector on j-th blade
$\underline{x}_j^\mathrm{gen}$	Generalised displacement of j-th blade
$\underline{(\ )}$	Complex quantity
$\underline{(\ )}^*$	Conjugate complex quantity
$\overline{(\ )}$	
β_m	Interblade phase angle of m-th mode
δ_m	Decay rate of m-th mode
$\underline{\Gamma}$	Mistuning matrix
$\underline{\gamma}_k$	Complex DFT of mistuning pattern
$\underline{\Psi}_m$	Vector of m-th sector mode shape
$\overline{\Psi}^B$	Average blade mode shape
$\hat{\Psi}_\mathrm{Meas}$	Calibration factor of generalised displacement
$\Phi_{m,j}$	Vector of m-th mode on j-th blade
Φ	Modal matrix of nominal system modes
ρ_m	Modeshape scaling factor of m-th mode
$\omega_{0,m}$	Undamped natural frequency of m-th mode
Ω	Excitation Frequency

ABBREVIATIONS

BTT	Blade tip timing
BTW	Backward travelling wave
CFD	Computational fluid dynamics
DFT	Discrete Fourier transform
FE	Finite element
FRF	Frequency response function
FTW	Forward travelling wave
IBPA	Interblade phase angle
SNM	Subset of nominal system modes
TWM	Travelling wave mode

GENERAL DEFINITIONS

The aim of the paper is to develop an approach that can be applied to measurement data without the necessity of any additional data, e.g. from a representative finite element (FE) model. During the derivation of the model equations it will be made use of a terminology similar to that of cyclic symmetric FE models.

Cyclic Symmetry

Subject of interest are rotors with N sectors. The $j = 1...N$ sectors or blades are numbered in the direction of its rotation. The rotor is assumed to be weakly damped and its mass is sufficiently high compared with the surrounding air, i.e. the eigenvectors of the undamped and uncoupled system are almost identical to the damped and coupled ones. Furthermore, a blade dominated mode family is regarded, i.e. there are $m = 1...N$ system modes in the frequency range of the regarded mode family. Each system mode is characterised by an interblade phase angle $\beta_m = 2\pi k(m)/N$, a travelling wave mode (TWM) index $k(m)$, a natural frequency $\omega_{0,m}$, a modal damping δ_m and a complex valued system mode shape vector $\underline{\Phi}_m$. Furthermore, the system modes are assumed to be mass-normalised, and hence, the reduction of the system's global mass matrix $\mathbf{M}_\mathrm{glob}$ and stiffness matrix $\mathbf{K}_\mathrm{glob}$ yields:

$$\underline{\Phi}_m^{*T}\mathbf{M}_\mathrm{glob}\underline{\Phi}_m = 1 \qquad \text{and} \qquad \underline{\Phi}_m^{*T}\mathbf{K}_\mathrm{glob}\underline{\Phi}_m = \omega_{0,m}^2 \quad (1)$$

Please note that an underline indicates a complex quantity and the asterisk its conjugate complex. The global mass and stiffness matrices are regarded in a disassembled state, i.e. the degrees of freedom at the sector interfaces are doubled and the periodic constraint needs to be satisfied by the system's eigenvectors. This allows to express $\mathbf{K}_\mathrm{glob}$ (and $\mathbf{M}_\mathrm{glob}$) by matrices $\mathbf{K}_{\mathrm{sec},j}$ (and $\mathbf{M}_{\mathrm{sec},j}$) derived from a sector model with free periodic interfaces:

$$\mathbf{K}_\mathrm{glob} = \mathrm{diag}\left\{\mathbf{K}_{\mathrm{sec},j}\right\} \quad (2)$$

The displacement vectors on the j-th blade are regarded in a local blade individual coordinate system, such that all sector matrices are identical and the sector index can be omitted, $\mathbf{K}_{\mathrm{sec},j} \equiv \mathbf{K}_\mathrm{sec}$ (and $\mathbf{M}_{\mathrm{sec},j} \equiv \mathbf{M}_\mathrm{sec}$). Furthermore, the m-th global system mode shape vector on the j-th blade $\underline{\Phi}_{m,j}$ can

be derived from the complex valued m-th sector mode shape vector $\underline{\Psi}_m$ via:

$$\underline{\Phi}_{m,j} = \underline{\Psi}_m \mathrm{e}^{-i\beta_m j} \tag{3}$$

The IBPA $\beta_m = 2\pi k(m)/N$ is a function of its respective TWM index $k(m)$. The TWM indices are assumed to be ordered from negative to positive TWMs:

$$k(m) = k_{\min}, \ldots, -1, 0, 1, \ldots, k_{\max} \tag{4}$$

with the maximum (and minimum) TWM index:

$$\begin{aligned} &k_{\max} = N/2, \;\; k_{\min} = -N/2+1 \text{ for even } N \quad \text{and} \\ &k_{\max} = (N-1)/2, \;\; k_{\min} = -k_{\max} \text{ for odd } N \end{aligned} \tag{5}$$

Since the $j = 1...N$ sectors are numbered in the direction of rotation, a negative TWM index k implies a backward travelling wave (BTW) whereas a positive index indicates a forward travelling wave (FTW) with respect to the direction of rotation. For $k(m) = 0$ (and $k(m) = N/2$ in the case of even N) the system mode is a standing wave with real sector mode shape vector Ψ_m. For a pair (m,n) of a double mode the respective TWMs with similar natural frequency ($\omega_{0,m} = \omega_{0,n}$) and nodal diameter ($|k(m)| = |k(n)|$) but opposite direction of rotation ($\beta_m = -\beta_n$) have conjugate complex sector mode shape vectors:

$$\omega_{0,m} = \omega_{0,n} \text{ and } \beta_m = -\beta_n \Longrightarrow \underline{\Psi}_m = \underline{\Psi}_n^* \tag{6}$$

Later on, it will be made use of the following relation that is derived from eq. (1) by using eq. (2) and eq. (3):

$$\begin{aligned} \omega_{0,m}^2 &= \underline{\Phi}_m^{*T} \mathbf{K}_{\mathrm{glob}} \underline{\Phi}_m = \sum_{j=1}^{N} \mathrm{e}^{i\beta_m j} \underline{\Psi}_m^{*T} K_{\mathrm{sec}} \underline{\Psi}_m \mathrm{e}^{-i\beta_m j} \\ \omega_{0,m}^2 &= N \underline{\Psi}_m^{*T} K_{\mathrm{sec}} \underline{\Psi}_m \end{aligned} \tag{7}$$

Complex Discrete Fourier Transform

Within this manuscript it will be made use of the complex discrete Fourier transformation (DFT) of input vectors $\mathbf{y}$ with $j = 1...N$ elements. The vector of the complex DFT of $\mathbf{y}$ is denoted by $\tilde{\mathbf{y}}$ and also a vector with N elements. The Fourier component $\underline{\tilde{y}}_k$ corresponding to the k-th wave number is defined by:

$$\underline{\tilde{y}}_k = \frac{1}{N} \sum_{j=1}^{N} y_j \mathrm{e}^{i\frac{2\pi k j}{N}} \qquad \text{with } k \in [k_{\min}, k_{\max}] \tag{8}$$

The complex DFT can be computed by a matrix vector multiplication with the help of the $N \times N$ Fourier matrix $\underline{\mathbf{E}}$:

$$\tilde{\underline{\mathbf{y}}} = [\underline{\tilde{y}}_{k_{\min}} \cdots \underline{\tilde{y}}_0 \cdots \underline{\tilde{y}}_{k_{\max}}]^T = \frac{1}{N} \underline{\mathbf{E}} \mathbf{y} \tag{9}$$

$$\mathbf{y} = \underline{\mathbf{E}}^{*T} \tilde{\underline{\mathbf{y}}} \tag{10}$$

$$\underline{\mathbf{E}} = \{\underline{E}_{mj}\} \qquad \text{with } \underline{E}_{mj} = \mathrm{e}^{i\beta_m j} \tag{11}$$

Equations of Motion in the Modal Domain

Subject of interest is the forced response of a cyclic symmetric rotor exposed to a harmonic excitation with the excitation frequency Ω in the vicinity of the frequency range of a blade dominated mode family. Consequently, the force vector $\mathbf{f}_j(t)$ on blade j as well as the blade individual responses $\mathbf{x}_j(t)$ are harmonic:

$$\mathbf{f}_j(t) = \Re\{\hat{\underline{\mathbf{f}}}_j \mathrm{e}^{i\Omega t}\} \tag{12}$$

$$\mathbf{x}_j(t) = \Re\{\hat{\underline{\mathbf{x}}}_j \mathrm{e}^{i\Omega t}\} \tag{13}$$

The forced response problem in blade individual coordinates reads:

$$[\mathbf{K}_{\mathrm{glob}} + i\Omega \mathbf{D}_{\mathrm{glob}} - \Omega^2 \mathbf{M}_{\mathrm{glob}}] \begin{bmatrix} \hat{\underline{\mathbf{x}}}_1 \\ \vdots \\ \hat{\underline{\mathbf{x}}}_N \end{bmatrix} = \begin{bmatrix} \hat{\underline{\mathbf{f}}}_1 \\ \vdots \\ \hat{\underline{\mathbf{f}}}_N \end{bmatrix} \tag{14}$$

Please note, that the formulation above makes use of disassembled global matrices, i.e. these equations are only valid, if the blade individual responses satisfy an additional constraint of matching displacements at the periodic interfaces. In the following the blade individual response is going to be expanded as a superposition of system modes, that are required to satisfy the periodic constraints. The natural frequencies of other system modes (than those of the studied blade mode family with $m = 1...N$ system modes) are assumed to be sufficiently far away from the studied frequency range, such that the blade individual response can be expanded as superposition of the studied system modes:

$$\hat{\underline{\mathbf{x}}}_j = \sum_{m=1}^{N} \hat{\underline{q}}_m \underline{\Phi}_{m,j} \tag{15}$$

$$\begin{bmatrix} \hat{\underline{\mathbf{x}}}_1 \\ \vdots \\ \hat{\underline{\mathbf{x}}}_N \end{bmatrix} = \begin{bmatrix} \underline{\Phi}_{1,1} & \cdots & \underline{\Phi}_{N,1} \\ \vdots & \ldots & \vdots \\ \underline{\Phi}_{1,N} & \cdots & \underline{\Phi}_{N,N} \end{bmatrix} \begin{bmatrix} \hat{\underline{q}}_1 \\ \vdots \\ \hat{\underline{q}}_N \end{bmatrix} = \underline{\Phi} \hat{\underline{\mathbf{q}}} \tag{16}$$

Assuming an individual (e.g. aerodynamic) damping level δ_m for each of the system modes, the global damping matrix is defined by:

$$\mathbf{D}_{\mathrm{glob}} = \mathbf{M}_{\mathrm{glob}} \underline{\Phi} \begin{bmatrix} 2\delta_1 & 0 & \ldots \\ 0 & \ddots & \vdots \\ \ldots & 0 & 2\delta_N \end{bmatrix} \underline{\Phi}^{*T} \mathbf{M}_{\mathrm{glob}} \tag{17}$$

Finally, the m-th line of the equations of motion for the tuned rotor reads in the modal domain:

$$(\omega_{0,m}^2 - \Omega^2 + 2i\Omega\delta_m)\hat{\underline{q}}_m = \sum_{j=1}^{N} \underline{\Phi}_{m,j}^{*T} \hat{\underline{\mathbf{f}}}_j = \hat{\underline{f}}_m^{\text{modal}} \tag{18}$$

Mistuning Model

Considering a limited accuracy of the manufacturing process, material inhomogeneities or wear, the properties of each rotor sector will differ from the reference:

$$\mathbf{M}_{\text{sec},j} = \mathbf{M}_{\text{sec}} + \Delta\mathbf{M}_j \tag{19}$$

$$\mathbf{K}_{\text{sec},j} = \mathbf{K}_{\text{sec}} + \Delta\mathbf{K}_j \tag{20}$$

The actual source of the mistuning shall be of minor interest and the focus is on an adequate modelling of the effect on the vibrational behaviour. Thus, all effects are concatenated in a change of the stiffness of the sector. Furthermore, the idea of the subset of nominal system modes (SNM) [10] comes along with the assumption that the perturbation matrices are scaled versions of the nominal stiffness matrix with scaling factor c_j:

$$\mathbf{K}_{\text{sec},j} = (1 + c_j)\mathbf{K}_{\text{sec}} \tag{21}$$

This leads to the coupled $N \times N$ system of equations for the mistuned rotor:

$$\left[\text{diag}\{\omega_{0,m}^2 - \Omega^2 + 2i\Omega\delta_m\} + \underline{\Gamma}\right] \hat{\underline{\mathbf{q}}} = \hat{\underline{\mathbf{f}}}^{\text{modal}} \tag{22}$$

The structure of the fully populated mistuning matrix $\underline{\Gamma}$ is given by:

$$\underline{\Gamma} = \{\underline{\Gamma}_{mn}\} = \underline{\Phi}^{*T}\,\text{diag}\{c_j\}\underline{\Phi} \qquad \text{with} \tag{23}$$

$$\underline{\Gamma}_{mn} = \sum_{j=1}^{N} c_j \underline{\Phi}_{m,j}^{*T} \mathbf{K}_{\text{sec}} \underline{\Phi}_{m,j} \tag{24}$$

Making use of the representation with sector modes $\underline{\Psi}_m$, see eq. (3), the elements of $\underline{\Gamma}$ read:

$$\underline{\Gamma}_{mn} = \sum_{j=1}^{N} c_j \mathrm{e}^{i\beta_m j} \underline{\Psi}_m^{*T} \mathbf{K}_{\text{sec}} \underline{\Psi}_n \mathrm{e}^{-i\beta_n j} \tag{25}$$

$$= \underline{\Psi}_m^{*T} \mathbf{K}_{\text{sec}} \underline{\Psi}_n \sum_{j=1}^{N} c_j \mathrm{e}^{i\frac{2\pi}{N}(k(m)-k(n))j} \tag{26}$$

Introducing the complex DFT $\underline{\gamma}_k$ of the stiffness scaling factors c_j according to eq. (8) and taking into account that $k(m) - k(n) \equiv m - n$ due to ordering of the modes, the elements of the mistuning matrix become:

$$\underline{\gamma}_k = \frac{1}{N} \sum_{j=1}^{N} c_j \mathrm{e}^{i\frac{2\pi k j}{N}} \tag{27}$$

$$\underline{\Gamma}_{mn} = N \underline{\Psi}_m^{*T} \mathbf{K}_{\text{sec}} \underline{\Psi}_n \underline{\gamma}_{m-n} \tag{28}$$

Approximation of the Sector Modes

For a pure blade mode without any disk participation the approximation of the sector modes by a scaled average blade mode $\overline{\Psi}^B$ reads:

$$\underline{\Psi}_m \approx \rho_m \overline{\Psi}^B \tag{29}$$

The approximation above is similar to the assumption made during the derivation of the FMM [1]. Inserting this into (7) yields:

$$\omega_{0,m} = \rho_m \sqrt{N \overline{\Psi}^{BT} \mathbf{K}_{\text{sec}} \overline{\Psi}^B} = \rho_m \omega_B \tag{30}$$

$$\Longrightarrow \omega_{0,m} = \frac{\rho_m}{\rho_n}\omega_{0,n} \quad \text{or} \quad \omega_{0,n} = \frac{\rho_n}{\rho_m}\omega_{0,m} \tag{31}$$

Using the above assumptions the elements of the mistuning matrix become:

$$\begin{aligned} \underline{\Gamma}_{mn} &= N \underline{\Psi}_m^{*T} \mathbf{K}_{\text{sec}} \underline{\Psi}_n \underline{\gamma}_{m-n} = \rho_m \rho_n \omega_B^2 \underline{\gamma}_{m-n} \\ &= \omega_{0,m}\omega_{0,n}\underline{\gamma}_{m-n} \end{aligned} \tag{32}$$

Measurement of Generalised Displacements

Unfortunately, it is impossible to measure the modal participation factors $\hat{\underline{q}}_m(\Omega)$ directly. Instead, it is assumed that a generalised displacement is measured which is based on a projection of the average blade mode $\overline{\Psi}^B$ to a scalar value. This projection is referred to $\hat{\Psi}_{\text{Meas}}$ and is scaled with the mode individual ρ_m and $\hat{\underline{q}}_m$. As a result one gets a generalised scalar displacement $\hat{\underline{x}}_j^{\text{gen}}$ per blade:

$$\hat{\underline{x}}_j^{\text{gen}} = \sum_{m=1}^{N} \hat{\underline{q}}_m \rho_m \hat{\Psi}_{\text{Meas}} \mathrm{e}^{-i\frac{2\pi k(m) j}{N}} \tag{33}$$

Introducing the abbreviation $\overline{\underline{q}}_m = \hat{\underline{q}}_m \rho_m \hat{\Psi}_{\text{Meas}}$ yields:

$$\begin{aligned} \hat{\underline{x}}_j^{\text{gen}} &= \sum_{m=1}^{N} \overline{\underline{q}}_m \mathrm{e}^{-i\frac{2\pi k(m) j}{N}} \\ \hat{\underline{\mathbf{x}}}^{gen} &= \underline{\mathbf{E}}^{*T} \overline{\underline{\mathbf{q}}} \Longrightarrow \overline{\underline{\mathbf{q}}} = \frac{1}{N}\underline{\mathbf{E}}\hat{\underline{\mathbf{x}}}^{gen} \end{aligned} \tag{34}$$

Hence, $\overline{\underline{\mathbf{q}}}$ can be identified as the complex DFT (or TWM expansion respectively) of the measured generalised displacements. Finally, the relation between measured generalised displacement $\hat{\underline{\mathbf{x}}}^{gen}$ and modal amplitudes $\hat{\underline{\mathbf{q}}}$ in the TWM domain reads:

$$\hat{\underline{\mathbf{q}}} = \text{diag}\{1/(\rho_m \hat{\Psi}_{\text{Meas}})\}\overline{\underline{\mathbf{q}}} \tag{35}$$

$$= \frac{1}{N}\text{diag}\{1/(\rho_m \hat{\Psi}_{\text{Meas}})\}\underline{\mathbf{E}}\hat{\underline{\mathbf{x}}}^{gen} \tag{36}$$

LINEAR IDENTIFICATION APPROACH

This section aims at introducing a novel linear least approach for the identification of system properties of turbomachinery components. This approach is based on a measured forced response sweep through a resonance of a blade dominated mode family that provides a set of measured frequency response functions (FRFs) of the generalised displacement $\hat{\underline{\mathbf{x}}}^{gen}(\Omega_s)$. These FRFs are available for $s = 1...N_\mathrm{f}$ distinct frequencies and have to contain amplitude and phase information for each of the N blades of the assembly. According to eq. (34) this set is transformed into its TWM expansion $\overline{\underline{\mathbf{q}}}(\Omega_s)$ which serves as the input data set. No further information is needed by the approach.

Governing Equations

Replacing the modal amplitudes $\hat{\underline{\mathbf{q}}}$ in (22) by the TWM expansion of the generalised displacement $\overline{\underline{\mathbf{q}}}$ yields:

$$\left[\mathrm{diag}\{\frac{\omega_{0,m}^2 - \Omega^2 + 2i\Omega\delta_m}{\rho_m \hat{\Psi}_\mathrm{Meas}}\} + \underline{\Gamma}\mathrm{diag}\{\frac{1}{\rho_m \hat{\Psi}_\mathrm{Meas}}\}\right]\overline{\underline{\mathbf{q}}} = \hat{\underline{\mathbf{f}}}^\mathrm{modal} \tag{37}$$

Multiplying each line with $\rho_m \hat{\Psi}_\mathrm{Meas}$ and using the assumption (32) as well as relation (31) yields:

$$\left[\mathrm{diag}\{\omega_{0,m}^2 - \Omega^2 + 2i\Omega\delta_m\} + \underline{\Gamma}'\right]\overline{\underline{\mathbf{q}}} = \mathrm{diag}\{\rho_m \hat{\Psi}_\mathrm{Meas}\}\hat{\underline{\mathbf{f}}}^\mathrm{modal} \tag{38}$$

$$\text{with} \quad \underline{\Gamma}'_{mn} = \frac{\rho_m \omega_{0,m}\omega_{0,n}\underline{\gamma}_{m-n}}{\rho_n} = \omega_{0,m}^2 \underline{\gamma}_{m-n} \tag{39}$$

In order to keep the approach linear, the mistuning matrix $\underline{\Gamma}'$ is approximated by $\overline{\underline{\Gamma}}$. Therefore, the entries in the mistuning matrix are replaced by the approximation:

$$\omega_{0,m}^2 \underline{\gamma}_{m-n} \approx \omega_{0,ref}^2 \underline{\gamma}_{m-n} = \overline{\underline{\gamma}}_{m-n} = \overline{\underline{\Gamma}}_{mn} \tag{40}$$

The relation above uses a reference frequency, that may be the identified frequency of the system mode with maximum nodal diameter for example. For small mistuning the relative sector frequency deviation Δf_j can be calculated from the identified $\overline{\underline{\gamma}}_k$ by:

$$\Delta f_j \approx \frac{1}{2}c_j = \frac{1}{2\omega_{0,ref}^2}\sum_{k=1}^{N}\overline{\underline{\gamma}}_k \mathrm{e}^{-i\frac{2\pi kj}{N}} = \frac{1}{2}\sum_{k=1}^{N}\underline{\gamma}_k \mathrm{e}^{-i\frac{2\pi kj}{N}} \tag{41}$$

If the least squares problem is solved iteratively, the simplification $\omega_{0,m} \approx \omega_{0,ref}$ may be replaced by the estimation of the system's frequencies of the last iteration yielding a slightly more realistic coupling behaviour. Finally, with the generalised modal force $\hat{\underline{f}}'_m = \rho_m \hat{\Psi}_\mathrm{Meas}\hat{\underline{f}}_m^\mathrm{modal}$ the governing system of linear equations reads:

$$\left[\mathrm{diag}\{\omega_{0,m}^2 - \Omega^2 + 2i\Omega\delta_m\} + \overline{\underline{\Gamma}}\right]\overline{\underline{\mathbf{q}}} = \hat{\underline{\mathbf{f}}}' \tag{42}$$

Least Squares Problem

The governing equations above are still arranged in an usual way where the system's parameters are given and the TWM expansion of the generalised displacements is unknown. However, the aim of the approach is to identify the system's parameter for a given measured response. Hence, the governing equations are now rearranged to isolate the unknown natural frequencies $\omega_{0,m}^2$, damping δ_m, mistuning $\overline{\underline{\gamma}}_k$ and forcing $\hat{\underline{f}}'_m$. For a fixed excitation frequency Ω_s one gets a $N \times (4N)$ system of complex equations:

$$\underline{\mathbf{L}}_s \begin{bmatrix}\mathbf{w}\\ \mathbf{d}\\ \underline{\mathbf{g}}\\ \overline{\underline{\mathbf{f}}}\end{bmatrix} = \underline{\mathbf{r}}_s \quad \text{with} \tag{43}$$

$$\underline{\mathbf{L}}_s = \left[\underline{\mathbf{L}}_w(\Omega_s)\ \underline{\mathbf{L}}_d(\Omega_s)\ \underline{\mathbf{L}}_g(\Omega_s)\ \underline{\mathbf{L}}_f\right] \quad \text{and} \tag{44}$$

$$\underline{\mathbf{r}}_s = \begin{bmatrix}\Omega_s^2\overline{\underline{q}}_1(\Omega_s)\\ \vdots \\ \Omega_s^2\overline{\underline{q}}_N(\Omega_s)\end{bmatrix} \tag{45}$$

The elementary least squares matrices for the natural frequencies and damping are diagonal. In specific measurement situations the number of frequencies and damping values can be decreased by further assumptions, e.g. symmetric properties of BTW and FTW or the expansion of the damping as a Fourier series.

$$\underline{\mathbf{L}}_w(\Omega_s) = \begin{bmatrix}\ddots & & \mathbf{0}\\ & \overline{\underline{q}}_m(\Omega_s) & \\ \mathbf{0} & & \ddots\end{bmatrix} \qquad \mathbf{w} = \begin{bmatrix}\omega_{0,1}^2\\ \vdots \\ \omega_{0,N}^2\end{bmatrix} \tag{46}$$

$$\underline{\mathbf{L}}_d(\Omega_s) = \begin{bmatrix}\ddots & & \mathbf{0}\\ & 2i\Omega_s\overline{\underline{q}}_m(\Omega_s) & \\ \mathbf{0} & & \ddots\end{bmatrix} \qquad \mathbf{d} = \begin{bmatrix}\delta_1\\ \vdots \\ \delta_N\end{bmatrix} \tag{47}$$

The least squares matrix for the generalised forces is trivial:

$$\underline{\mathbf{L}}_f = \begin{bmatrix}\ddots & & \mathbf{0}\\ & -1 & \\ \mathbf{0} & & \ddots\end{bmatrix} \qquad \underline{\mathbf{f}} = \begin{bmatrix}\hat{\underline{f}}'_1\\ \vdots \\ \hat{\underline{f}}'_N\end{bmatrix} \tag{48}$$

Since the mistuning pattern is a real valued quantity, it holds $\overline{\underline{\gamma}}_k = \overline{\underline{\gamma}}_k^*$. Thus, the $\overline{\underline{\gamma}}_k$ with negative k are replaced by its respective counterparts with positive k. Thereby, the number of variables reduces significantly and reflects the fact, that a total number of N values (counting real and imaginary part separately) is sufficient to reproduce a real valued pattern of N values. Furthermore, the mean value $\overline{\underline{\gamma}}_0$ is set to zero.

A mean shift of all the system's frequencies is already captured by the identification of the $\omega_{0,m}$, i.e. the column of the least squares matrix corresponding to the average of the mistuning would be a linear combination of the columns of $\underline{\mathbf{L}}_w$. By omitting the mean value of the mistuning this rank-deficiency is avoided and one ends up with a total number of $N-1$ independent values (the real and imaginary parts of $\overline{\underline{\gamma}}_1$ to $\overline{\underline{\gamma}}_{k_{\max}}$) to be identified.

$$\underline{\mathbf{L}}_g(\Omega_s) = \{\underline{L}_{mn}\} \qquad \underline{\mathbf{g}} = \begin{bmatrix} \overline{\underline{\gamma}}_1 \\ \vdots \\ \overline{\underline{\gamma}}_{k_{\max}} \end{bmatrix} \tag{49}$$

$$\underline{L}_{mn} = \overline{\underline{q}}_{(m+n) \bmod N} + \overline{\underline{q}}^*_{(m-n) \bmod N} \tag{50}$$

Finally, the complete system consists of $N_\mathrm{f} \cdot N$ lines, since each of the N_f frequency lines of the discrete representation of the measured FRFs adds N lines to the least squares problem:

$$\begin{bmatrix} \underline{\mathbf{L}}_1 \\ \vdots \\ \underline{\mathbf{L}}_{N_\mathrm{f}} \end{bmatrix} \begin{bmatrix} \mathbf{w} \\ \mathbf{d} \\ \underline{\mathbf{g}} \\ \underline{\mathbf{f}} \end{bmatrix} = \begin{bmatrix} \underline{\mathbf{r}}_1 \\ \vdots \\ \underline{\mathbf{r}}_{N_\mathrm{f}} \end{bmatrix} \tag{51}$$

To prepare eq. (51) for a numerical solution, the complex unknowns as well as the equations are split in their respective real and imaginary parts. Afterwards, the real valued least squares problem is solved by standard numerical libraries.

Assessment of the Quality of the Identification

In order to enable an assessment of the validity of the identified parameters, a residual is calculated for each of the TWMs. Therefore, the following norm is used:

$$||\underline{q}|| = \frac{1}{N_\mathrm{f}} \sum_{s=1}^{N_\mathrm{f}} \underline{q}(\Omega_s) \underline{q}^*(\Omega_s) \tag{52}$$

The identified modal parameters are used to build the system of linear equations (42). By solving this system a reconstruction $\overline{\underline{q}}_k^{\mathrm{recon}}(\Omega_s)$ of the input FRFs is generated. The residual of the k-th TWM is defined as the norm of the difference of reconstruction and input FRF divided by the norm of the input FRF:

$$\frac{||\overline{\underline{q}}_k - \overline{\underline{q}}_k^{\mathrm{recon}}||}{||\overline{\underline{q}}_k||} \tag{53}$$

Minimum Example Demonstrating the Basic Idea

To demonstrate the basic idea and study fundamental sources of disturbances a single degree of freedom oscillator is regarded:

$$(\omega_0^2 - \Omega^2 + 2i\Omega\delta)\underline{q} = \underline{f} \tag{54}$$

We assume a measurement of the response $\underline{q}(\Omega_s) = q_\mathrm{r}(\Omega_s) + iq_\mathrm{i}(\Omega_s)$ subject to a harmonic excitation $\underline{f}\mathrm{e}^{i\Omega t}$ with $\underline{f} = f_\mathrm{r} + if_\mathrm{i}$. Equation (54) and the force is split into real and imaginary part and the system is rearranged to separate the unknowns:

$$\begin{aligned} \mathrm{I}: \quad & q_\mathrm{r}(\Omega_s)\omega_0^2 - 2\Omega_s q_\mathrm{i}(\Omega_s)\delta - f_\mathrm{r} = \Omega_s^2 q_\mathrm{r}(\Omega_s) \\ \mathrm{II}: \quad & q_\mathrm{i}(\Omega_s)\omega_0^2 + 2\Omega_s q_\mathrm{r}(\Omega_s)\delta - f_\mathrm{i} = \Omega_s^2 q_\mathrm{i}(\Omega_s) \end{aligned} \tag{55}$$

The complete real valued linear least squares system then reads:

$$\begin{bmatrix} q_\mathrm{r}(\Omega_1) & -2\Omega_1 q_\mathrm{i}(\Omega_1) & -1 & 0 \\ q_\mathrm{i}(\Omega_1) & 2\Omega_1 q_\mathrm{r}(\Omega_1) & 0 & -1 \\ \vdots & \vdots & \vdots & \vdots \\ q_\mathrm{r}(\Omega_{N_\mathrm{f}}) & -2\Omega_{N_\mathrm{f}} q_\mathrm{i}(\Omega_{N_\mathrm{f}}) & -1 & 0 \\ q_\mathrm{i}(\Omega_{N_\mathrm{f}}) & 2\Omega_{N_\mathrm{f}} q_\mathrm{r}(\Omega_{N_\mathrm{f}}) & 0 & -1 \end{bmatrix} \begin{bmatrix} \omega_0^2 \\ \delta \\ f_R \\ f_I \end{bmatrix} = \begin{bmatrix} \Omega_1^2 q_\mathrm{r}(\Omega_1) \\ \Omega_1^2 q_\mathrm{i}(\Omega_1) \\ \vdots \\ \Omega_{N_\mathrm{f}}^2 q_\mathrm{r}(\Omega_{N_\mathrm{f}}) \\ \Omega_{N_\mathrm{f}}^2 q_\mathrm{i}(\Omega_{N_\mathrm{f}}) \end{bmatrix} \tag{56}$$

It may be emphasised that the above $2N_\mathrm{f} \times 4$ system (eq. (56)) is linear. Hence, no initial guess of the frequency, force or damping level is needed and the solution is unique. Furthermore, the solution of such a linear least squares problem can be computed very efficiently even for thousands of measured frequency lines.

Now the focus is on the influence of missing or erroneous measurement data on the identification approach. Therefore, three different cases are analysed. Case A takes into account incomplete but perfect input data. Case B considers measurement noise with a noise to signal ratio of 10 percent and case C studies the slight impact of a different mode that is not modelled.

Figure 1 shows the clean reference data compared with the input data used for the identification approach in the cases A-C. The relative error of the identified natural frequency and damping is quantified in table 1. In the absence of any disturbances the approach perfectly identifies the system's modal parameters. This even holds, if only a small part of the resonance sweep through is provided, see fig. 1a). The presence of noise in the input data (see fig. 1b)) leads to an underestimation of the damping (-9.4%) and a relative frequency error of 5.4%, compare table 1. Especially the damping error increases rapidly when the noise ratio is further increased, see also fig. 2.

Besides the susceptibility to noise a severe impact of slight systematic errors can also be observed. Case C considers a superposed response of another mode at a normalised frequency of 1.75. As a consequence the real and imaginary part of the FRF get a little systematic shift, compare fig. 1c), and the identified damping is affected significantly. Whereas the frequency error is only 0.7%, the damping is overestimated by 35.5%, see table 1.

Hence, the approach needs to be stabilised to reach the desired goal of a quantification of the system's damping.

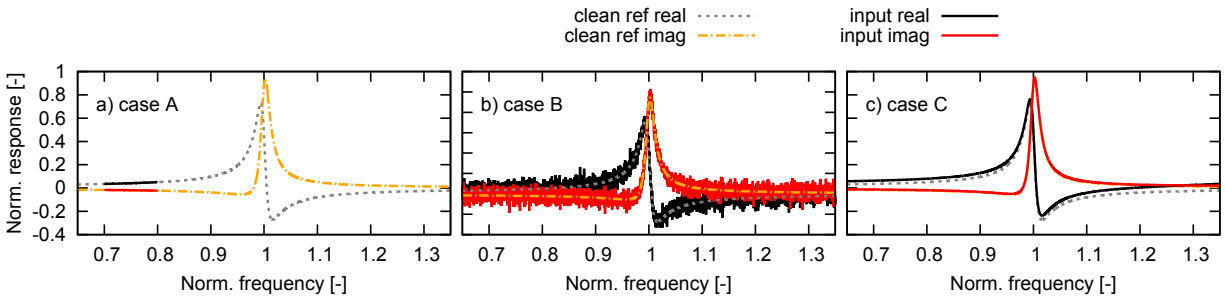

FIGURE 1. Visualisation of the input data: a) case A with incomplete data; b) case B with noisy data; c) case C with a slight response of a second mode superposed

case	rel. error of identified	
	frequency	damping
A (incomplete data)	≈ 0	≈ 0
B (noisy data)	5.39%	-9.42%
C (2nd mode superposed)	-0.707%	35.49%

TABLE 1. Impact of incomplete and erroneous input data on the identified frequency and damping

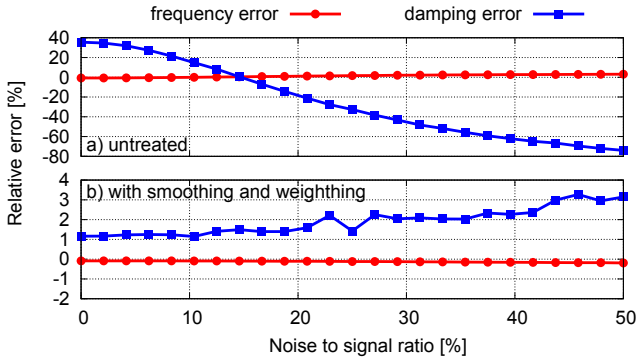

FIGURE 2. Relative damping and frequency error as a function of the noise to signal ratio for case C with the influence of a second mode plus superposed noise. The errors are based on an identification with: a) untreated data; b) smoothing and weighting

STABILISATION TECHNIQUES

The previous investigations revealed a severe susceptibility of the identified damping to noisy or generally erroneous data. This section aims at providing some ideas to overcome this drawback.

Smoothing and Weighting

In order to remove noise from the data, real and imaginary parts of the FRFs may be smoothed prior to the identification. There are many suitable techniques available for the purpose of removing uncorrelated noise, e.g. moving averages or higher order polynomial filters. This implementation of the approach makes use of a cubic regression spline with a given number of support points. The second issue identified by the study of the simplified example above is the high susceptibility to systematic errors like the slight shift introduced by the second off-resonant mode. To overcome this drawback, a weighting technique may be applied. Such a technique applies a high penalty to errors that occur in the vicinity of the resonance and a much lower penalty to errors occurring in the off-resonant frequency regime. A simple weighting function may be built based on the amplitude of the smoothed FRFs. Figure 2 shows the stabilising effect of smoothing and weighting compared with the application of the untreated data. Therefore, case C has been studied with an overlaid noise of different strengths.

Reduction of Unknowns

In order to stabilise the fit further, the number of unknowns can be reduced by additional simplifications or assumptions. During rotation it is often valid to assume the excitation of a single TWM. Furthermore, according to the concept of aerodynamic influence coefficients the impact of just a few adjacent blades is often sufficient to characterise the aerodynamic damping behaviour. Hence, the damping of the system modes can be expanded by a Fourier series with fewer DOFs. In specific situations, e.g. standstill measurements, it may be valid to assume that some or all of the modal properties of the system are symmetric with respect to the TWM index, i.e. frequencies and/or damping values of system modes are only a function of the absolute value of the TWM index and forward and backward travelling wave modes have identical properties. The symmetry assumption can also be combined with the harmonic expansion to reduce the DOFs even further. Finally, standstill measurements with single point excitation on one of the blades allow the assumption of a certain phasing of the modal force. At least the modal forces of TWMs with opposite direction of rotation have to be conjugate complex.
Figure 3 gives an overview of the complete identification process with the major steps necessary to extract the natural frequencies, damping and mistuning from measured generalised displacements of every blade.

SIMULATED BENCHMARKS CASES

Typical applications of the identification approach may be experimental modal analyses (EMA) at standstill and vibration measurements under rotation. An application of the approach to a simulated validation case as well as real mea-

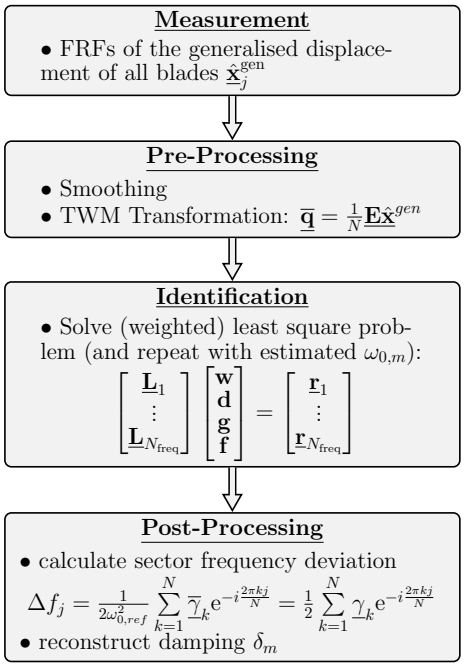

FIGURE 3. Flow chart of the identification process

surement cases of experimental modal analyses at standstill can be found in the second part of the paper [11]. The scope of this part is limited to vibrations under operating conditions. Since the approach relies on measured FRFs of each blade, the most obvious application are BTT measurements of an integral resonance crossing.

Case 1: Rotor at Design Speed With Constant Modal Damping and Single Travelling Wave Mode Excitation

Before the approach is applied to BTT datasets, the SNM approach shall be compared to a finite element (FE) model of the complete rotor. To enable a comparison of the SNM response with a whole assembly FE model in a reasonable time scale a coarse grid representation of the investigated research rotor is built and constant modal damping is assumed. Figure 4a) shows the coarse mesh of the whole assembly FE model and 4b) shows contours of the investigated 1st blade mode family on the sector model. Subject of interest is the 2nd stage blisk rotor of a high pressure compressor research rig, that has been subject of other investigations [12]. The rotor has 28 blades and is studied at its design speed. Whereas centrifugal loads, the Coriolis effect and a constant temperature load are taken into account, the effect of the pressure load on the airfoil is omitted. The used implementation of the SNM approach is able to take into account gyroscopic effects. Figure 5a) shows the good match of the tuned natural frequencies of the system modes predicted by the SNM and the FE model as a function of the nodal diameter. Due to the Coriolis effect, forward (FTW) and backward travelling waves (BTW) have different natural frequencies. The relative split of the FTW and BTW are depicted in fig. 5b). To demonstrate the mistuned forced response capabilities of the SNM both models are mistuned by scaling the stiffness of the sectors according to a mistuning pattern that has been identified in a measurement of the respective blade mode family, see [12]. The force is applied at a single node of each blade's tip and an arbitrary excitation of the TWM -8 is chosen. The applied physical force in the finite element model has been used to calculate an equivalent modal force of the SNM. Figure 5c) shows the almost perfect agreement of SNM and FE model exemplarily for the tip displacement of blade 1.

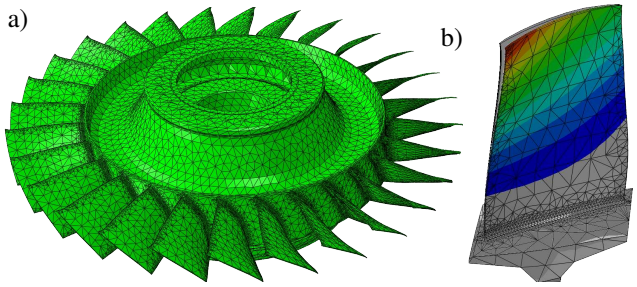

FIGURE 4. Illustration of the investigated research rotor: a) coarse FE model for the validation of the SNM approach including Coriolis effects; b) corresponding sector model with contours of the studied 1st blade mode family

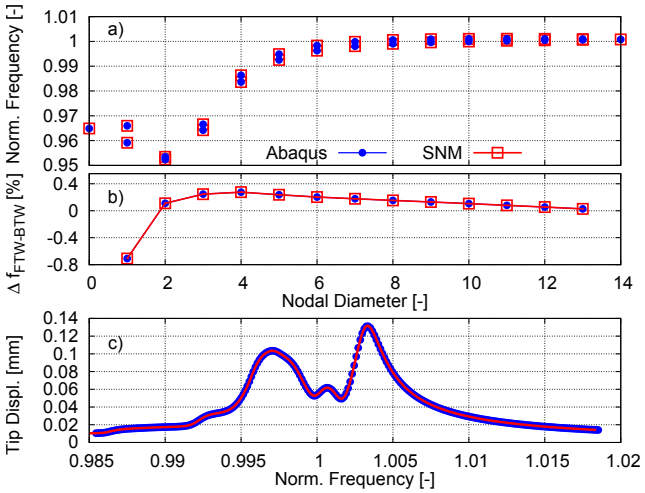

FIGURE 5. Comparison of the FE model with the SNM approach for the 1st blade mode family: a) normalised natural frequency vs. nodal diameter; b) relative frequency split of FTW to BTW due to the Coriolis effect at design speed; c) tip displacement of blade 1 vs. frequency for TWM -8 excitation

Next, the derived forced response data is transformed into the TWM domain and the identification approach has been applied to this first generic test case. Since the input data is of perfect quality, smoothing and weighting has been omitted. The number of unknowns has been reduced by two assumptions. It has been taken into account that only a TWM -8 force is expected and the decay rates δ_m are assumed to be constant. A second iteration has been performed after the first solution of the least squares problem. In this second iteration the scaling of the mistuning with the constant ref-

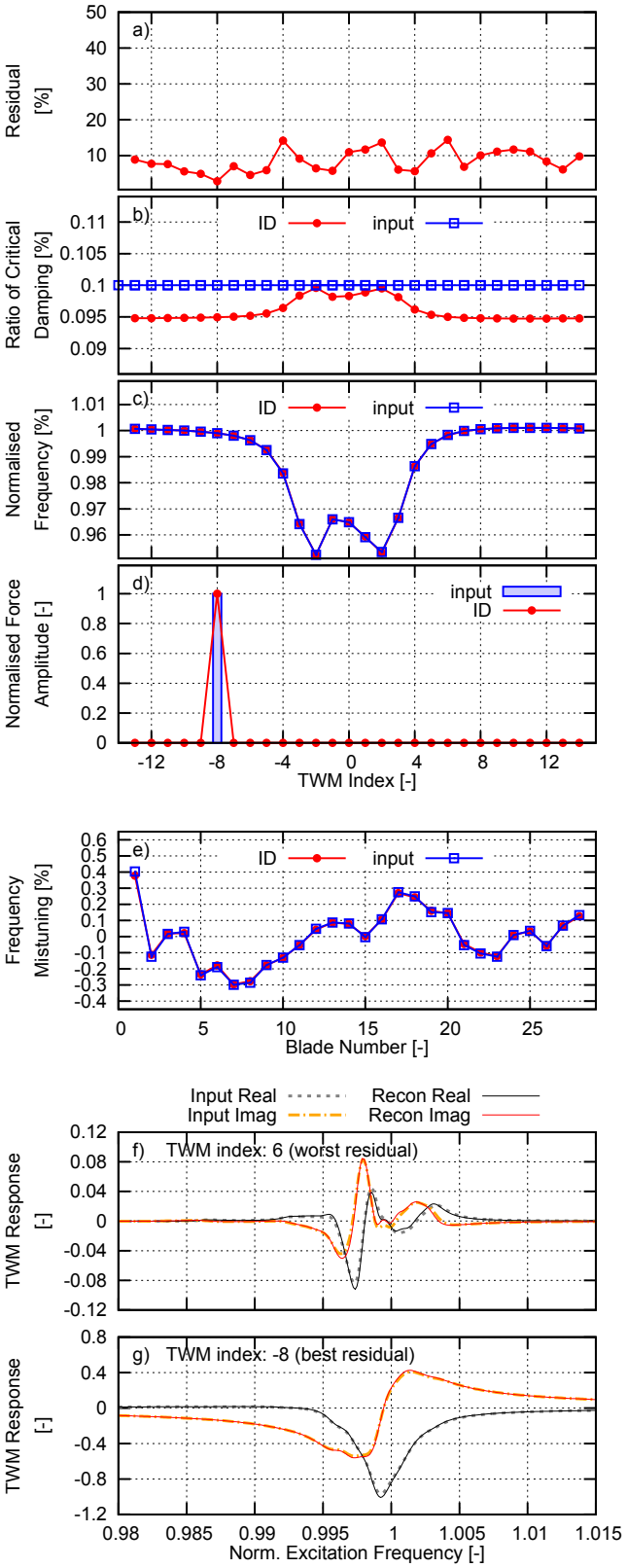

FIGURE 6. Output of the identification approach for case 1: a) residuals; b) damping; c) system frequencies; d) force amplitude vs. TWM index; e) mistuning vs. blade number, and reconstructed and input FRF of TWM with worst residual f) and best residual g)

erence frequency $\omega_{0,\mathrm{ref}}$ has been replaced by the identified $\omega_{0,m}$ of the first iteration yielding a coupling behaviour that is closer to the stiffness adjusted models. The output of the approach is depicted in fig. 6a)-f). Figure 6a) shows the residual defined in eq. (53) for each of the TWM indices. With an average residual of $\approx 8\%$ and a maximum residual of $\approx 15\%$ the identified parameters can be assumed to be trustworthy. The largest discrepancy can be noticed for the damping with a maximum error of $\approx 5\%$, see fig. 6b).
The system frequencies and thereby the split of FTW and BTW due to the Coriolis effect are perfectly identified by the approach, see fig. 6c). Thus, the approach is able to shed light on the possible presence of gyroscopic effects in real hardware. Figure 6e) shows the perfect agreement of the identified mistuning pattern with the pattern applied to the analytical model. Finally, figs. 6f)-g) illustrate the good quality of the identification by comparing the reconstructed FRFs with the input data for the best (6g)) and worst (6f)) matching FRF.

Case 2: Simulated BTT Measurement With Aerodynamic Damping, Coriolis Effect and Multiple TWMs excited

Whereas the preceding study directly made use of the simulated data of the tip displacements, the next test case goes a step further and aims at validating the complete post-processing chain involved in vibration measurements under rotating conditions. Since the approach needs FRFs of all blades of the studied rotor, BTT data sets are most obvious to be suitable for the approach. To proof the suitability it will be made use of a BTT simulation environment based on the SNM representation. This high fidelity BTT simulation environment is able to take into account a plurality of physical phenomena present in measurements of real hardware, e.g. static deflection, noise and blade or BTT probe positioning errors. Furthermore, it has been validated against real engine data, see [13] for a detailed description of the functionality and the validation. The used BTT configuration is similar to the one used in the rig test, compare [13]. In a first step, noise and systematic probe positioning errors are neglected and it shall be tested, if the approach can be applied to FRFs derived from the BTT software in case of perfect measurement conditions. Therefore, an acceleration of the rotor with an integral resonance crossing of a low engine order with the frequency of the 1st blade mode family is simulated. In addition to the gyroscopic effect and the arbitrarily chosen excitation of the TWM -8 further model features are taken into account, e.g. static deflection of the blades, aerodynamic damping and further weak excitations of other TWMs besides the dominant TWM -8. The chosen aerodynamic damping curve is assumed to be representative of 1st flap modes of front rotors of high pressure compressors, see 7b) for an illustration. Aerodynamic stiffness is also included, but its effect on the aeroelastic eigenfrequencies is much lower compared to the gyroscopic effect. To test the approach with respect to the identification of any irregularities in the force distribution a few weak force components have been added to TWMs -13,-3 and +3. Those

can be the result of rotor-stator interactions (Tyler-Sofrin modes) for example.

After the BTT data sets (time of arrivals) have been generated by the SNM, the BTT software derives deflection data for each of the blades. Figure 8 shows the raw deflection of blade 1 perceived by the BTT software with static deflection and blade vibration clearly visible. The static deflection predicted by the FE model has been amplified by a factor of 5 to be a bit more pronounced. The excitation has been scaled to produce a deflection of ≈ 1 mm from peak to peak. Based on the expected engine order and a number of revolutions (block width of the fit), the BTT software performs a least squares fit and produces FRFs of each blade. Figure 9 shows real and imaginary part of such a derived FRF by the BTT software exemplarily for blade 1. These FRFs of a generalised displacement represent the input data for the identification approach.

In contrast to the preceding case, some settings of the identification approach have been altered. No specific TWM forcing is assumed and hence, each of the TWM force components is identified. The damping curve is expanded as a Fourier series with 10 harmonics. The least squares problem is solved repeatedly and the matrix is updated with the latest prediction of the system frequencies in the coupling terms. Furthermore, a weighting technique has been used to stabilise the damping prediction for such a high number of parameters (20). The weighting function is based on the amplitude of the fit (to produce a higher penalty for errors near a resonance peak) and the residual of the last iteration (to make the approach reduce bad residuals at the cost of a slightly worse match on other TWMs). After a few iterations ($<$10) the residuals do not improve further and the process is stopped.

Figure 7a)-g) shows the final output of the identification approach. The residuals are very low with values below 5% and hence, the identified parameters can be assumed to be trustworthy. The lower residuals compared to the first case are due to the higher damping level (factor of 10) which smooths out errors in the coupling of the TWMs due to the simplified model of the mistuning matrix. The mistuning and the system's tuned natural frequencies with the impact of the Coriolis effect are perfectly identified by the approach. Also, the approach identified the smooth aerodynamic damping curve very accurately from the data though it has had degrees of freedom to produce an arbitrary degenerated shape. Additionally, the forces of the excited TWMs have been identified properly with a correct amplitude ratio. Hence, the approach can also be applied without any assumption on the excited TWM index and is able to recognise any irregularities in the excitation spectrum. Finally, the comparison of reconstructed and input FRFs shows the expected good match indicated by the low residuals, see figs. 7f)-g).

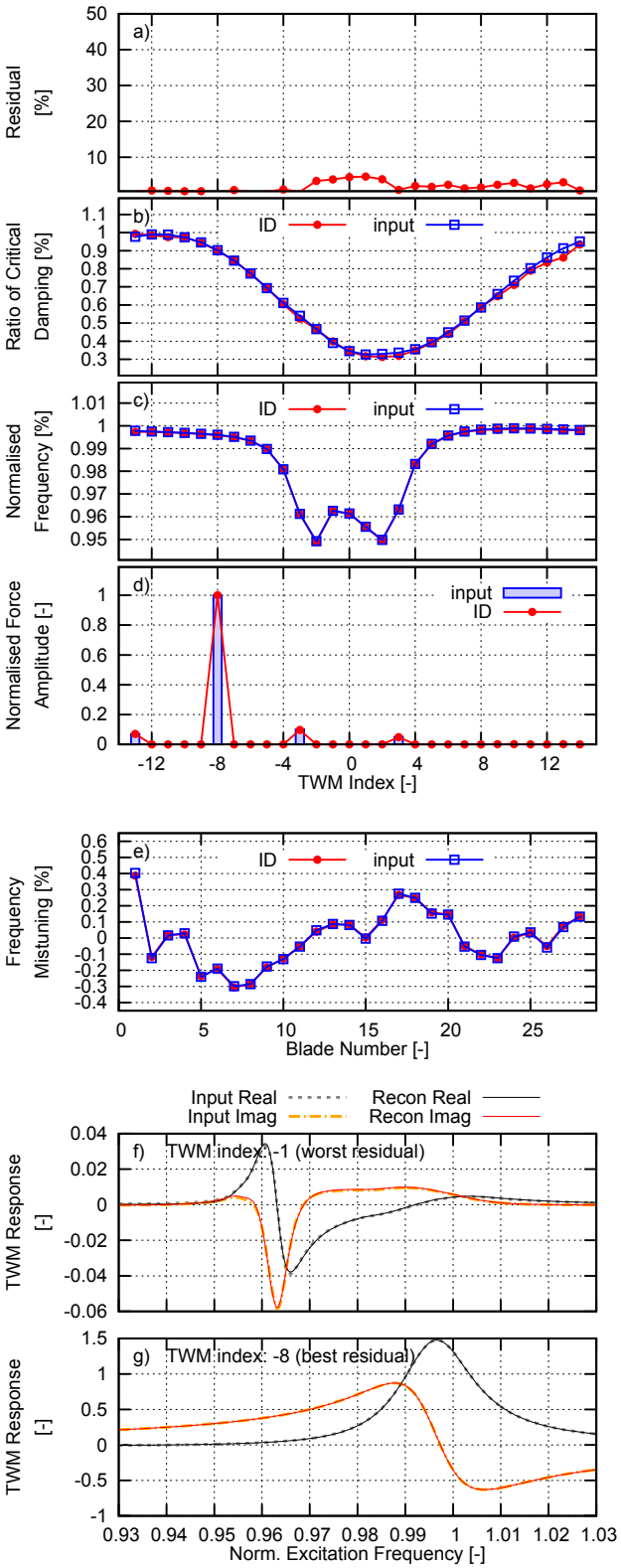

FIGURE 7. Output of the identification approach for case 2: a) residuals; b) damping; c) system frequencies; d) force amplitude vs. TWM index; e) mistuning vs. blade number, and reconstructed and input FRF of TWM with worst residual f) and best residual g)

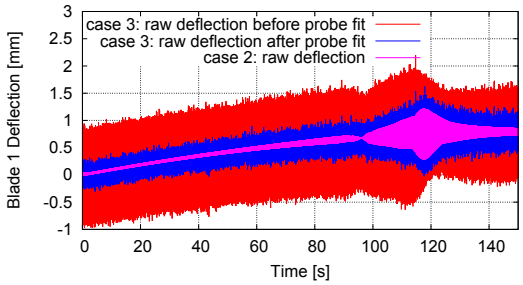

FIGURE 8. Comparison of the blade 1 deflection perceived by the BTT software for the clean case 2 and the noisy case 3 with additional probe positioning error

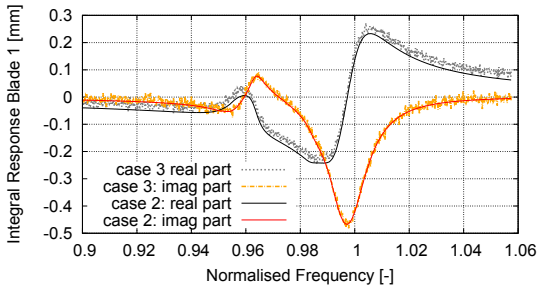

FIGURE 9. Comparison of the integral blade 1 response determined by the BTT software for the clean case 2 and the noisy case 3 with additional probe positioning error

Case 3: Simulated BTT Measurement With Additional Probe Positioning Error and Noise

As a last validation step the preceding case is now going to be disturbed by typical errors occurring during BTT measurements of real engine hardware. Therefore, sensor noise in the detection of time of arrivals (with the once per revolution sensor as well as with the BTT probes) and systematic probe positioning errors, i.e. deviations of the actual axial and/or circumferential position of the BTT probes compared to the used BTT configuration, are taken into account. The applied probe positioning errors are similar to those identified in the rig test of the studied rotor, compare [13]. The noise in the time of arrivals has been adjusted to produce a noise level that is 40% of the maximum blade deflection. As a result the raw deflection before the probe fit perceived by the BTT software is largely dominated by the introduced error, see fig. 8. After a fit of the probe positions at the beginning of the acceleration the BTT software is able to reduce the errors and the remaining deflection signal is composed of the blade vibration and noise, see also fig. 8. The majority of the noise is removed within the derivation of the FRFs with the BTT software due to the least squares fit over a number of revolutions (20 in this particular case), see fig. 9. Nevertheless, some noise remains and also a slight shift of the real part of the FRF can be noticed when comparing the FRFs with the ones derived in case 2, see fig. 9. This shift is a relict of the assumption of vanishing vibration at the beginning of the acceleration within the fit of the BTT probe positions and is equivalent to the observed influence of a second mode within case C of the minimum example, com-

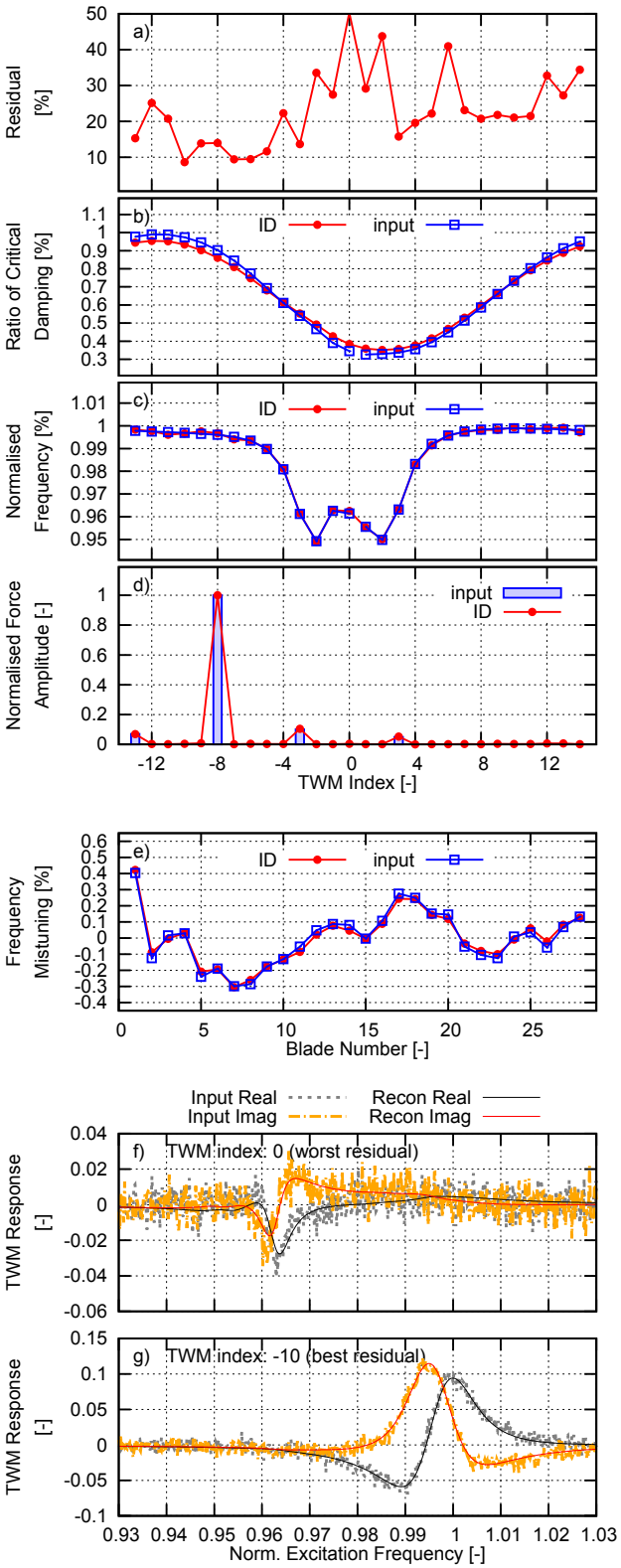

FIGURE 10. Output of the identification approach for case 3: a) residuals; b) damping; c) system frequencies; d) force amplitude vs. TWM index; e) mistuning vs. blade number, and reconstructed and input FRF of TWM with worst residual f) and best residual g)

pare fig. 1c). Within the study of the minimum example it has been already revealed that the identified damping is very sensitive to such errors. Hence, weighting becomes very important when the approach is applied to realistic BTT data and the shape of the damping curve needs to be restricted to a smooth one with only a few harmonics (aerodynamic influence coefficients) considered. In this case, the number of harmonics has been reduced to 2, i.e. only the influence of 2 adjacent blades is taken into account from an aeroelastic point of view.
Figure 10 shows the output of the identification approach for the realistic data set compared with the input. It is obvious that the residuals increase significantly up to 50%. The average residual is still low with $\approx 20\%$. From fig. 10f)-g) it can be noticed, that the high residual is due to the fact, that on some TWMs the response is much lower than on others and as a result the noise to signal ratio as well as the residual is much higher. Furthermore, fig. 10f) shows, that the reconstruction is still meaningful, i.e. the peak in the model coincides with a peak in the response. All in all, the identified modal parameters can be assumed to be trustworthy. This indication is confirmed by comparing the identified parameters with the input data, see figs. 10b)-e). The system frequencies including gyroscopic effects, the aerodynamic damping curve, the multitude of TWM forces and the mistuning pattern have been successfully extracted from the realistic engine representative BTT data set.

CONCLUDING REMARKS

A novel linear least squares approach for the identification of the system's properties of a mistuned rotor has been presented. The approach is based on measured FRFs of each blade and aims at extracting:

- tuned natural frequencies of system modes as a function of the TWM index;
- tuned overall damping ratios (structural + aerodynamic) as a function of the IBPA;
- the mistuning pattern;
- and the force amplitudes of the TWMs.

Studies with simulated datasets of different fidelity (SDOF up to realistic BTT data) revealed that the approach suffers from noise and systematic errors, but can be stabilized by a smoothing and weighting technique as well as a restriction to a certain number of AICs for the aerodynamic damping. This is no major restriction, since in many cases it turns out that only a few AICs are relevant. Thus, the approach enables the extraction of the relevant system properties in an engine representative environment and can help identifying root causes for possible discrepancies between prediction and observation. The most obvious application under rotating conditions are BTT measurements which are an affordable state of the art measurement technique to monitor the vibration response of every single blade of a rotor. Hence, the approach extends the state of the art in the measurement of system properties of mistuned bladed rotors under operating conditions, which is of enormous value for the validation of CFD, FE and aeromechanical reduced order models.

REFERENCES

[1] Feiner, D. M.; Griffin, J. H., 2002. "A Fundamental Model of Mistuning for a Single Family of Modes". In ASME Paper No. GT2002-30425.

[2] Feiner, D. M.; Griffin, J. H., 2003. "Mistuning Identification of Bladed Disks Using a Fundamental Mistuning Model—Part I: Theory". In ASME Paper No. GT2003-38952.

[3] Feiner, D. M.; Griffin, J. H., 2003. "Mistuning Identification of Bladed Disks Using a Fundamental Mistuning Model—Part II: Application". In ASME Paper No. GT2003-38953.

[4] Kuehhorn A.; Beirow B., 2010. "Method for Determining Blade Mistuning on Integrally Manufactured Rotor Wheels". *Patent US 2010/0286934 A1*.

[5] Kaszynski, A. A., Beck, J. A., and Brown, J. M., 2014. "Automated Finite Element Model Mesh Updating Scheme Applicable to Mistuning Analysis". In ASME Paper No. GT2014-26925.

[6] Maywald, T., Backhaus, T., Schrape, S., and Kühhorn, A., 2017. "Geometric Model Update of Blisks and its Experimental Validation for a Wide Frequency Range". In ASME Paper No. GT2017-63446.

[7] Huang, Y., Dimitriadis, G., Kielb, R. E., and Li, J., 2017. "System Eigenvalue Identification of Mistuned Bladed Disks Using Least-Squares Complex Frequency-Domain Method". In ASME Paper No. GT2017-63008.

[8] Fransson, T., and Verdon, J., 1992. "Updated Report on Standard Configurations for Unsteady Flow Through Vibrating Axial-flow Turbomachine Cascades". *CT Technical Rept. LTT-CONF-1991-005*.

[9] Schönenborn, H., Chenaux, V., and Ott, P., 2011. "Aeroelasticity at Reversed Flow Conditions: Part 1—Numerical and Experimental Investigations of a Compressor Cascade With Controlled Vibration". In ASME Paper No. GT2011-45034.

[10] Yang, M. T., and Griffin, J. H., 2001. "A Reduced-Order Model of Mistuning Using a Subset of Nominal System Modes". *Journal of Engineering for Gas Turbines and Power,* ***123***(4), pp. 893–900.

[11] Beirow, B., Figaschewsky, F., and Kühhorn, A., 2018. "An Inverse Approach to Identify Tuned Aerodynamic Damping, System Frequencies and Mistuning. Part 2: Application to Blisks at Rest". In Proceedings of the 15th ISUAAAT: Paper No. ISUAAAT15-021.

[12] Beirow, B., Kühhorn, A., Figaschewsky, F., Hönisch, P., Giersch, T., and Schrape, S., 2017. "Model Update and Validation of a Mistuned High Pressure Compressor Blisk". *Proceedings of the 23nd ISABE: Paper ISABE-2017-22568*.

[13] Figaschewsky, F., Hanschke, B., and Kühhorn, A., 2018. "Efficient Generation of Engine Representative Tip Timing Data Based on a Reduced Order Model for Bladed Rotors". In ASME Paper No. GT2018-76342.